

“New View” of Protein Folding Reconciled with the Old Through Multiple Unfolding Simulations

Themis Lazaridis and Martin Karplus*

Twenty-four molecular dynamics trajectories of chymotrypsin inhibitor 2 provide a direct demonstration of the diversity of unfolding pathways. Comparison with experiments suggests that the transition state region for folding and unfolding occurs early with only 25 percent of the native contacts and that the root-mean-square deviations between contributing structures can be as large as 15 angstroms. Nevertheless, a statistically preferred unfolding pathway emerges from the simulations; disruption of tertiary interactions between the helix and a two-stranded portion of the β sheet is the primary unfolding event. The results suggest a synthesis of the “new” and the classical view of protein folding with a preferred pathway on a funnel-like average energy surface.

A “new view” of protein folding (1) that postulates many ways of reaching the native state is replacing the specific pathway concept attributed to Levinthal (2). In the new view, a general bias of the energy surface toward the native state reduces the search problem so that folding can occur on the experimental time scale without invoking specific pathways. This view is based on statistical mechanical models (3–5) and lattice simulations (5–8), but there is little direct experimental evidence for its validity. In this report we present results obtained from 24 unfolding trajectories of chymotrypsin inhibitor 2 (CI2) (Fig. 1). CI2 is of particular interest for such simulations because it is a small fast-folding protein, it has been studied experimentally by protein engineering methods, and it exhibits two-state behavior with the same transition state for folding and unfolding (9, 10). Molecular dynamics simulations were performed with the CHARMM program (11), a polar hydrogen model for the protein (11, 12), and an implicit model for the solvent (13–15); the latter reduces the required computer time by more than an order of magnitude relative to that for simulations with explicit water molecules (16, 17). Although the trajectories show very diverse behavior, they have common structural features that define an average unfolding pathway.

The radius of gyration (R_g) and the root-mean-square deviation (rms) from the crystal structure vary widely as a function of time (Fig. 2A). For example, trajectory 16 (Tr16) exhibits a single concerted increase in rms and R_g to reach a denatured state, whereas Tr11 shows more complex behavior with the oscillations of both rms and R_g

increasing as a function of time. The rms deviation is plotted against the radius of gyration R_g for the same set of trajectories to remove the effect of the distribution in unfolding times expected for any unimolecular reaction (that is, corresponding events could occur at different times in different trajectories) (Fig. 2B). The diversity in the trajectories is still present. Some trajectories (such as Tr1) show a simple approximately simultaneous increase in R_g and rms near the native state and much more complexity after partial denaturation, whereas others (such as Tr11 and Tr16) have complex behavior near the native state.

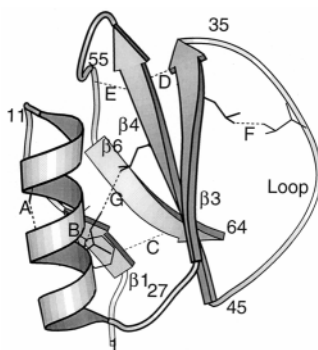


Fig. 1. Representation of the structure of CI2; the drawing was made with the Molscript program (35). The structural elements are defined as follows: strand $\beta 1$, residues 1 to 11; helix, residues 12 to 26; strand $\beta 3$, residues 27 to 33; loop, residues 34 to 44; strand $\beta 4$, residues 45 to 53; strand $\beta 6$, residues 54 to 64; for simplicity, strands $\beta 2$ and $\beta 5$, which consist of only two and four residues, respectively, are not shown [see (10, 14)]. One contact from each of the seven groups used to analyze the secondary and tertiary structure formed along the trajectories is indicated. The seven groups correspond to main-chain contacts in the helix (A: Val¹⁹-N, Glu¹⁵-O); $\beta 1$ to helix (B: Trp⁵-CE2, Ile²⁰-CG1); $\beta 1$ to $\beta 4$, $\beta 6$ (C: Val⁶³-N, Thr³-O); $\beta 3$ to $\beta 4$ (D: Val⁵¹-N, Leu³²-O); $\beta 4$ to $\beta 6$ (E: Ala⁵⁸-N, Phe⁵⁰-O); loop and minicore contacts (F: Leu³²-CD1, Val³⁸-CG1); helix to $\beta 3$, $\beta 4$, $\beta 6$ (G: Ile²⁰-CD, Leu⁴⁹-CD2).

The time dependence of 52 native contacts provides a measure of the change in structure during unfolding (Fig. 3); the types of contacts that are included are indicated (Fig. 1). Their use is analogous to the choice of the fraction of the native contacts, Q , as the progress variable in lattice simulations, and we use the designation Q here (3, 7, 18). In the late stages of unfolding (early stages of folding; $Q = 0.25$ to 0.3) most contacts are absent or are present only a small fraction of the time and only a few exist for more than 80% of the time. For $Q \cong 0.5$, most contacts are present part of the time and there is a broad, relatively uniform distribution of native contact probabilities. Clearly, the system is becoming more compact but very diverse sets of structures are still being sampled. For $Q \cong 0.75$, most of the contacts exist for more than 60% of the time, with a small number having a probability of less than 40%; they are contacts involving the $\beta 1$ strand or the long loop (Fig. 1).

The effective energy (intraprotein energy plus solvation free energy from the implicit solvent model) as a function of the number of contacts, averaged over all the trajectories,

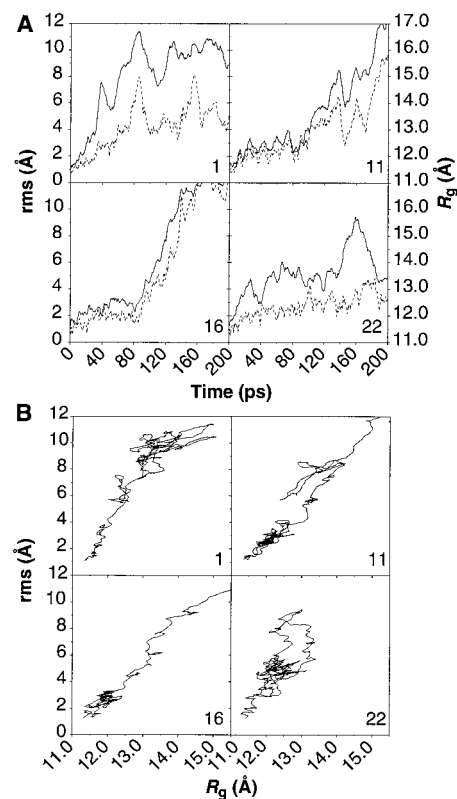


Fig. 2. (A) Backbone rms from the crystal structure of CI2 and radius of gyration R_g for four unfolding trajectories as a function of time; rms values are shown as a solid line with a scale on the vertical axis on the left; R_g values are shown as a dotted line with a scale on the vertical axis on the right. (B) Root mean square versus R_g for the same trajectories.

T. Lazaridis, Department of Chemistry and Chemical Biology, Harvard University, Cambridge, MA 02138, USA. M. Karplus, Department of Chemistry and Chemical Biology, Harvard University, Cambridge, MA 02138, USA, and Laboratoire de Chimie Biophysique, ISIS, Institut le Bel, Université Louis Pasteur, 67000 Strasbourg, France.

*To whom correspondence should be addressed.

has a general funnel-like form (Fig. 4A) (19) as the polypeptide chain approaches the native structure. Similar behavior has been observed in folding simulations with lattice models for fast-folding sequences (7, 18, 19) and in an all-atom plus explicit solvent simulation of the free energy surface of a protein (20). The complex highly nonmonotonic variation in the effective energy as a function of Q (Fig. 4B) or of the time (Fig. 4C) in the individual trajectories contrasts sharply with the average funnel-like behavior and suggests that care is required in interpreting the latter. This is in accord with the fact that it has not been possible to refold a protein with an all-atom model either by low temperature dynamics (21) or by simulated annealing (22).

The evolution of the contacts (Fig. 3) can be related directly to specific structural changes (Fig. 5). In spite of the diversity of the unfolding trajectories (Fig. 2), there is a certain commonality in the disappearance of different structural features (Fig. 5B). After early displacement of the $\beta 1$ strand, a key event is disruption of the hydrophobic core formed primarily by side chains of the residues of the α helix and of strands $\beta 3$ and $\beta 4$. The disappearance of the core occurred simultaneously with the destruction of the helix or the $\beta 3$ - $\beta 4$ sheet or both in some trajectories; in other trajectories, the secondary structural elements persisted after the core was disrupted (Fig. 5A) (23). The contacts between the helix and these strands (h, $\beta 3$ - $\beta 4$), the other major β -

strand contacts ($\beta 4$ - $\beta 6$), and the loop contacts show intermediate stability.

The most detailed experimental data on the structural changes in CI2 during folding and unfolding are provided by protein-engineering experiments (10, 24). In such experiments, measurements are made of the ratio Φ of the effect of a mutation on the folding rate to that on the stability of the native state. If $\Phi = 1$ for a given residue, the transition state is presumed to have a structure that is very similar to the native state in the neighborhood of that residue; if $\Phi = 0$, it is presumed that the transition state is like the denatured state in that region. Intermediate values of Φ are more complicated to interpret (10, 25). Itzhaki *et al.* (10) found that most residues (with a few important exceptions; see below) have Φ values between 0.2 and 0.3. From our simulations [see also discussion in (25)], this suggests that the transition state consists of an ensemble of configurations with the number of native contacts equal to about 25% (Fig. 3). Thus, the transition region is made up of a wide range of structures with an average rms deviation of 9 Å (see above). Another measure of the position of the transition region is provided by the dependence of the equilibrium constant and the rate constant for folding on the concentration of a denaturant, such as guanidinium hydrochloride (Gdn-HCl). The standard interpretation of such data (26) is that the coefficient m describing the Gdn-HCl concentration dependence of a rate or equilibrium constant can be simply related

to the difference in exposed surface area in the two states involved (m for the unfolded state versus the native state and m_{k_f} for the unfolded state versus the transition state). The experimental value of m [$m = 1.80$ kcal/mol-M, where M refers to the concentration of the denaturant (26)] and the exposed surface area of the crystal structure leads to about 8500 Å² for the exposed surface area of the unfolded state (27); this value is equal to that obtained for the fully extended structure. The same calculation for the folding rate ($m_{k_f} = 1.14$ kcal/mol-M) yields about 5850 Å² for the transition state. This value corresponds to that from the simulations (~ 6000 Å²) when the fraction of native contacts Q is about 0.25, in agreement with the ensemble average interpretation of the Φ values given above. Values of $Q = 0.2$ and 0.3 have been assumed in other approaches to CI2 folding that made use of a statistical free energy functional (28) and lattice models (29), respectively.

Given the funnel-like form of the effective energy surface (Fig. 4), the transition state barrier must arise from an entropic bottleneck; that is, a decrease in entropy as a function of Q that is greater than the effective energy decrease, so that a free energy barrier is generated near $Q \cong 0.25$ when the early contacts are formed. Such a balance between the effective energy and the entropy is found in the high-temperature lattice simulations (7, 18) and also in an all-atom simulation of a

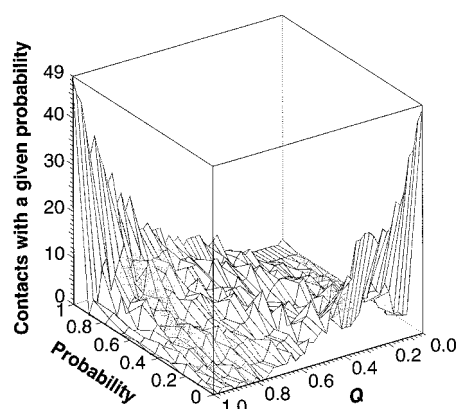


Fig. 3. Number of contacts with a given probability of being formed as a function of Q , the fraction of native contacts. Contacts are defined in Fig. 1. Results correspond to an average over the 24 trajectories. Two structures with $Q = 0.25$ can have rms values as large as 15 Å (average, 9 Å); at $Q = 0.5$, the maximum rms is 12 Å (average, 5.5 Å); and at $Q = 0.75$, the maximum rms is 3.2 Å (average, 1.8 Å). At low Q (early in folding), there are no native contacts with high probability. As Q increases, there are many contacts with low probability and a few with high probability. Only at large Q (late in folding) does the system fairly suddenly form most contacts with a high probability.

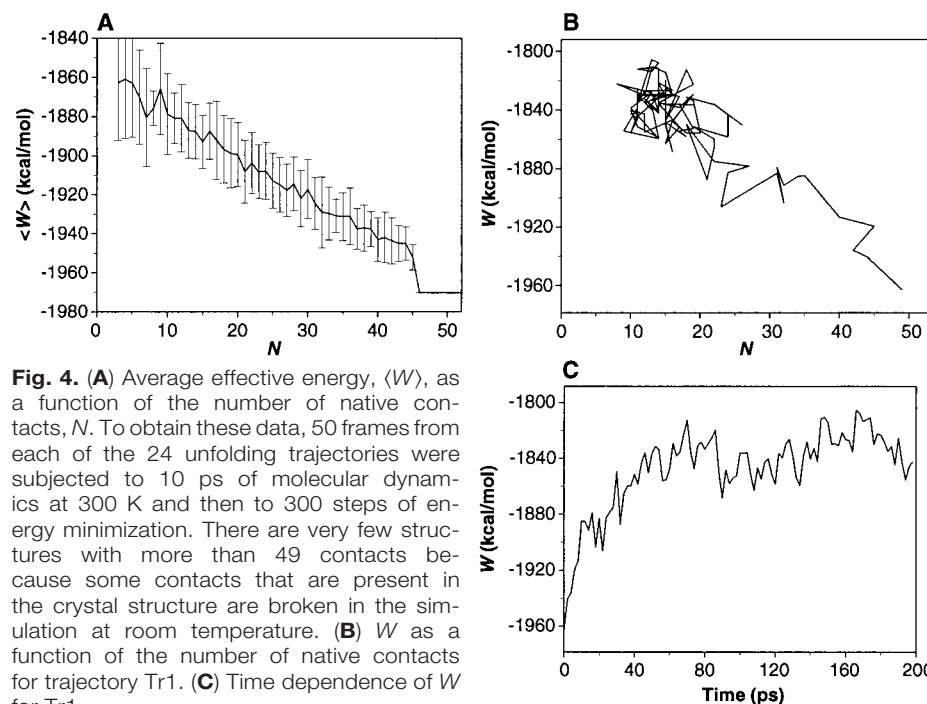


Fig. 4. (A) Average effective energy, $\langle W \rangle$, as a function of the number of native contacts, N . To obtain these data, 50 frames from each of the 24 unfolding trajectories were subjected to 10 ps of molecular dynamics at 300 K and then to 300 steps of energy minimization. There are very few structures with more than 49 contacts because some contacts that are present in the crystal structure are broken in the simulation at room temperature. (B) W as a function of the number of native contacts for trajectory Tr1. (C) Time dependence of W for Tr1.

three-helix bundle protein (20).

To obtain more insight into the structure of the transition state, it is of interest to consider certain hydrophobic residues that have experimental Φ values significantly larger than the average of $\Phi \sim 0.2$ to 0.3 (10). Most striking is residue Ala¹⁶ ($\Phi \cong 1.1$ for Ala¹⁶ \rightarrow Gly), which is part of the α helix. In these simulations, as in those of Li and Daggett (16), the number of contacts made by the Ala side chain was found to depend primarily on the presence of the helix and not on interactions with β strands. The value of $\Phi_{MD}(t)$, which is defined (16) as the ratio of the number of contacts at time t during the trajectory to that in the native state, remains between 0.8 and 1 as long as the α helix is present (30). The mutation of Val¹⁹ to Ala is characterized by a negative value of Φ ($\Phi = -0.3$); the negative value arises because both the folding and unfolding rates are greater in the mutant, whereas the native state is destabilized by the mutation. This result can be explained by the fact that this substitution destabilizes the protein because of loss of packing interactions, but it stabilizes the isolated helix because of the higher helix propensity of an Ala residue (31). The mutations Ala¹⁶ to Gly and Val¹⁹ to Ala are both consistent with a transition state that contains a partially formed helix. Leu⁴⁹ (experimental $\Phi \cong 0.5$) is involved in interactions between strand $\beta 3$ and the helix in the native structure. Analysis of $\Phi_{MD}(t)$ in our simulations and in those of Li and Daggett shows that $\Phi_{MD}(t)$ remains between 0.5 and 0.8 throughout most of the unfolding trajectories; many of the interactions are with other residues in the β strand, in accord with the conclusion from the simulations that the $\beta 3$ – $\beta 4$ sheet is present early in folding.

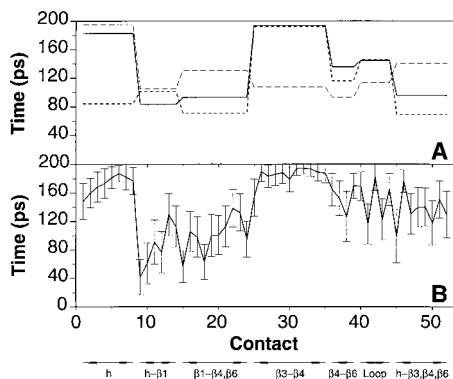


Fig. 5. (A) Average time each group of contacts last appears in three trajectories: —, a typical trajectory; ---, $\beta 3$ – $\beta 4$ contacts disappear early; - · -, α helix contacts disappear early. (B) Evolution of native contacts as a function of time. The average time each contact last appeared in the 24 trajectories is shown; bars = 1 SD.

The protein engineering experiments for CI2 have been interpreted in terms of a nucleation-condensation mechanism (32). Both the simulations and the experiments point to the helix, which has weak native-like interactions in the denatured state (25, 33), as an essential nucleation element. The rate-limiting step in the predominant pathway appears to be a coalescence of the $\beta 1$ strand and the helix with a few distant residues in the protein that leads to partial burial of the hydrophobic core. The simulations suggest that formation of the $\beta 3$ – $\beta 4$ sheet may also be involved in the nucleation; the most probable contacts for $Q = 0.25$, the putative transition region, are in the helix and in the $\beta 3$ – $\beta 4$ sheet (34). Once the nucleus is formed, the rest of the protein is expected to rapidly form the native structure (32).

The analysis of 24 CI2 trajectories has demonstrated that there exists a wide diversity in unfolding trajectories, in accord with the new view of protein folding. However, when the trajectories are analyzed in terms of the evolution of native contacts, a statistically predominant pathway emerges for this fast-folding protein. Thus, a strong preference for a certain order of events in the folding process, determined by the amino acid sequence, is compatible with a funnel-like (single global basin of attraction) average energy surface.

REFERENCES AND NOTES

- R. L. Baldwin, *Nature* **369**, 183 (1994).
- C. Levinthal, *J. Chim. Phys.* **65**, 44 (1968).
- J. C. Bryngelson and P. G. Wolynes, *J. Phys. Chem.* **93**, 6902 (1989).
- E. I. Shakhnovich and A. M. Gutin, *Biophys. Chem.* **34**, 187 (1989).
- M. Karplus and E. Shakhnovich, in *Protein Folding*, T. Creighton, Ed. (Freeman, New York, 1992), pp. 127–195.
- K. A. Dill *et al.*, *Protein Sci.* **4**, 561 (1995).
- M. Karplus and A. Šali, *Curr. Opin. Struct. Biol.* **5**, 58 (1995).
- D. Thirumalai and S. A. Woodson, *Accounts Chem. Res.* **29**, 433 (1996).
- S. E. Jackson and A. R. Fersht, *Biochemistry* **30**, 10428 (1991).
- L. S. Itzhaki, D. E. Otzen, A. R. Fersht, *J. Mol. Biol.* **254**, 260 (1995).
- B. R. Brooks *et al.*, *J. Comp. Chem.* **4**, 187 (1983).
- E. Neria, S. Fischer, M. Karplus, *J. Chem. Phys.* **105**, 1902 (1996).
- The solvation model assumes that the solvation free energy is given by the sum of group contributions: $\Delta G^{solv} = \sum_i \Delta G_i^{solv}$ with $\Delta G_i^{solv} = \Delta G_i^{ref} - \sum_j f_j(r_{ij})V_j$, where ΔG_i^{ref} is the solvation free energy of group i in a reference model compound, V_j is the volume of group j , and $f_j(r_{ij})$ is the solvation free energy density of group j at distance r_{ij} . Values of ΔG_i^{ref} are obtained from Privalov and Makhatadze [P. L. Privalov and G. I. Makhatadze, *J. Mol. Biol.* **232**, 660 (1993)] with slight modifications. The solvation free energy density is given by $f_j = 4\pi r_{ij}^2 = \alpha_j \exp(-x_{ij}^2)$ with $x_{ij} = (r_{ij} - r_{min,j})/\lambda_j$, where $r_{min,j}$ is the van der Waals radius of j and λ_j is a correlation length (3.5 Å for most groups). α_j is obtained from the solvation data making sure that the solvation free energy of deeply buried groups is zero. Ionic side chains are neutralized and a distance-dependent dielectric constant is used for the electrostatic interactions. Simulations of proteins with the implicit solvent model yield satisfactory structural and thermodynamic properties for proteins (such as stable native structures under physiological conditions and appropriate energetics for the unfolding transition). Further, use of the implicit solvent model for simulations of dynamics, as well as thermodynamics, is justified by barnase unfolding simulations with explicit solvent (17), which have demonstrated that solvation is essentially simultaneous with the exposure of groups in the interior of the protein. Details and tests of the model will be presented separately.
- The starting point for the simulations was the crystal structure of CI2 (PDB code 2ci2). Only residues 20 to 83 were modeled; the first 19 residues are disordered in the crystal and were not included in the simulations. Crystal water molecules were deleted. Hydrogen atoms were built with the HBUILD algorithm in CHARMM and 300 steps of energy minimization were performed by using the full potential followed by 50 ps of dynamics at 300 K. The 24 trajectories were started from the last structure obtained at 300 K. The only difference among the trajectories was the seed of the random number generator used to assign velocities corresponding to 500 K to the atoms at the beginning of each unfolding trajectory. The time step was 2 fs and the nonbonded interactions were updated every 20 steps. Coordinate frames were saved every 0.4 ps.
- As a test of the implicit solvent calculations, comparisons have been made with room temperature native and unfolding (498 K) simulations of Li and Daggett (16) that used a similar protein model and solvation with explicit water molecules. Analysis of the trajectories kindly provided by V. Daggett demonstrated that our results generally agree with their simulations. A 1.2-ns simulation of CI2 with the continuum solvent model at 300 K yielded an α carbon rms of 1.3 Å from the starting crystal structure; Li and Daggett found a value of 2.5 Å over 5.3 ns (1.5 Å if the flexible loop is excluded). The four unfolding trajectories of Li and Daggett show behavior similar to that reported here, although the time required for denaturation is longer. The increase in unfolding rate in our simulations is due, in part, to the absence of friction; this has been demonstrated by use of the continuum solvent model with Langevin dynamics and a friction coefficient corresponding to that of liquid H₂O (not shown).
- A. Li and V. Daggett, *J. Mol. Biol.* **257**, 412 (1996).
- A. Caffisch and M. Karplus, *J. Mol. Biol.* **252**, 672 (1995). In this simulation, there were about 9000 solvent atoms and 1100 protein atoms.
- A. Šali, E. Shakhnovich, M. Karplus, *Nature* **369**, 248 (1994).
- J. N. Onuchic, P. G. Wolynes, Z. Luthey-Schulten, N. D. Succi, *Proc. Natl. Acad. Sci. U.S.A.* **92**, 3626 (1995).
- E. M. Boczek and C. L. Brooks III, *Science* **269**, 393 (1995); Z. Guo, C. L. Brooks III, E. M. Boczek, *Proc. Natl. Acad. Sci. USA* **94**, 10161 (1997).
- D. O. Alonso and V. Daggett, *J. Mol. Biol.* **247**, 501 (1995).
- We have made a number of simulated annealing runs starting with the unfolded state and found that all of them become trapped far from the native state; the best result had a decrease in energy from -1909 to -1955 kcal/mol and a decrease in rms from 8.9 to 7.1 Å.
- The unfolding results of Li and Daggett (16) are very similar to those obtained here, except the $\beta 3$ – $\beta 4$ sheet appears to unfold somewhat earlier in the present simulations.
- J. L. Neira *et al.*, *Folding Design* **1**, 189 (1996).
- A. R. Fersht, *Curr. Opin. Struct. Biol.* **7**, 3 (1997).
- J. K. Myers, C. N. Pace, J. M. Scholtz, *Protein Sci.* **4**, 2138 (1995).
- All values given in this paragraph are for the truncated protein used in the simulations and the protein engineering experiments. The first 19 residues, which are disordered, are assumed to be fully exposed in both the native state and the denatured state of the complete protein used in the experiments described in (9), so that they make no contri-

- tribution to the change in surface area. The protein engineering experiments (10) used the truncated protein.
28. B. A. Schoemaker, J. Wang, P. G. Wolynes, *Proc. Natl. Acad. Sci. U.S.A.* **94**, 777 (1997).
29. J. N. Onuchic, N. D. Socci, Z. Luthey-Schulten, P. G. Wolynes, *Folding Design* **1**, 441 (1996).
30. Li and Daggett (16) focus on the value of $\Phi_{MD}(t)$ at a selected transition state. We have monitored $\Phi_{MD}(t)$ during the entire trajectory for some of the present simulations as well as those of Li and Daggett.
31. A. Chakrabarty, T. Kortemme, R. L. Baldwin, *Protein Sci.* **3**, 843 (1994).
32. A. R. Fersht, *Proc. Natl. Acad. Sci. U.S.A.* **92**, 10869 (1995).
33. B. Nölting *et al.*, *ibid.* **94**, 826 (1997).
34. There is a difference between the contact analysis from the simulations and the protein engineering ex-

periments; for example, the protein engineering experiments deal only with the effect of side-chain mutations, whereas the contact analysis of the simulations is based on main-chain interactions for secondary structure and on side-chain interactions for tertiary structure (Fig. 1).

35. P. J. Kraulis, *J. Appl. Crystallog.* **24**, 946 (1991).

7 July 1997; accepted 30 October 1997

Atomic and Macroscopic Reaction Rates of a Surface-Catalyzed Reaction

J. Wintterlin,* S. Völkening, T. V. W. Janssens, T. Zambelli, G. Ertl

The catalytic oxidation of carbon monoxide (CO) on a platinum (111) surface was studied by scanning tunneling microscopy. The adsorbed oxygen atoms and CO molecules were imaged with atomic resolution, and their reactions to carbon dioxide (CO₂) were monitored as functions of time. The results allowed the formulation of a rate law that takes the distribution of the reactants in separate domains into account. From temperature-dependent measurements, the kinetic parameters were obtained. Their values agree well with data from macroscopic measurements. In this way, a kinetic description of a chemical reaction was achieved that is based solely on the statistics of the underlying atomic processes.

Chemical kinetics—that is, the determination of rate equations as functions of macroscopic parameters like temperature, pressure, and concentrations—constitutes one of the main sources of information about the mechanisms of chemical reactions. An analysis of the kinetics is, however, connected with a fundamental problem—mentioned also in basic physical chemistry textbooks—that a reaction mechanism, the sequence of elementary steps by which a product is formed, cannot be uniquely established by kinetic measurements, because overlooked intermediate steps or other complications can never be ruled out (1). The reverse procedure, the derivation of the kinetics from a microscopic mechanism, is unique, allowing one to disprove possible microscopic models. As a means for a positive proof of a mechanism, reverse analysis has not been an option so far simply because the atomic scale was difficult to access experimentally. Here we present results of a study in which this reverse approach has been successfully pursued for a heterogeneous chemical reaction, the oxidation of CO molecules on a single-crystal Pt(111) surface. By means of scanning tunneling microscopy (STM), we resolved the reactants, observed their statistical reactions as functions of time, and derived a quantitative rate equation. The kinetic parameters thus obtained agree surprisingly well

with those from previous macroscopic measurements.

In several previous STM studies, qualitative mechanistic effects in chemical surface reactions could be identified, including site-specific reactivities, the formation of islands of the reactants, and in particular, effects of structural rearrangements of the metal substrate (reconstructions) (2–4). However, to our knowledge there have been no studies to date in which quantitative rate laws could be extracted from the atomically resolved surface processes (5) so that possible influences on the macroscopic kinetics is still an open question.

The oxidation of CO on Pt(111) was chosen here because it is a well-studied, model-like catalytic reaction (6, 7) and is relatively simple; it also represents the basis for the catalytic removal of CO from exhaust gases by oxidation on Pt surfaces. The reaction does not involve reconstructions and has been demonstrated to follow the so-called Langmuir-Hinshelwood mechanism (8), which generally underlies heterogeneous catalysis and assumes that the product is formed by reaction between the adsorbed reactants. In the present case, the reaction comprises the dissociative adsorption of oxygen (9), the molecular adsorption of CO (10), and the combination of the two surface-adsorbed species to CO₂ (8); the CO₂ molecules are immediately released into the gas phase (7, 11). There are, however, indications that the actual mechanism involves more complex features than this simple scheme: From temperature-

programmed desorption studies (12), it was concluded that the reacting adsorbed O atoms and CO molecules are not randomly distributed, but that the reaction takes place at the perimeters of oxygen islands. That the reactants in a surface reaction might be localized in separate domains is, in fact, a long-discussed notion for catalytic reactions in general, and effects on the kinetics have been predicted by simulations (13).

Despite the detailed knowledge of many features of the CO and O reaction on Pt(111), it is characteristic—and this holds also for most complex chemical processes such as catalytic reactions—that no mechanistic model exists that is fully consistent with all features of the kinetics, as is reflected by, for example, the coverage dependence of all of the reaction “constants” involved in the CO₂ production rates (6, 7). Also, the reaction at island edges was disputed on the basis of isotope mixing studies (14), which concluded a homogeneous reaction probability. A recent study on this subject (15) produced the unexpected result that oxygen atoms in the interior of islands are more reactive than isolated atoms.

Our investigations were performed in an ultrahigh-vacuum chamber with the use of a variable-temperature STM, which, along with the cleaning of the Pt sample, was described previously (16). The experiments concentrated on the surface reaction step $\text{CO}_{ad} + \text{O}_{ad} \rightarrow \text{CO}_2$ (ad, adsorbed). In order to monitor the progress of the reaction as a function of time, we cooled the Pt sample, reducing the reaction rate to fit the speed of the STM equipment. According to previous studies, the reaction starts well below room temperature (11, 12). Experiments were performed as “titration experiments,” by first covering the sample with submonolayers of oxygen atoms, which were then reacted off by exposure to constant CO pressures.

After preparation of the oxygen layer [Fig. 1, time (t) = 0], the oxygen atoms, which are imaged as dark dots [this is an electronic effect that has been predicted theoretically (17)], formed small islands, in agreement with previous observations (16). The periodic structure within the islands corresponded to the known (2×2) structure of chemisorbed oxygen atoms on Pt(111)

Fritz-Haber-Institut der Max-Planck-Gesellschaft, Faradayweg 4-6, D-14195 Berlin, Germany.

*To whom correspondence should be addressed.